Bioorganic Chemistry 85 (2019) 229–239

Contents lists available at ScienceDirect

Bioorganic Chemistry

journal homepage: www.elsevier.com/locate/bioorg

Docking- and pharmacophore-based virtual screening for the identification of novel *Mycobacterium tuberculosis* protein tyrosine phosphatase B (MptpB) inhibitor with a thiobarbiturate scaffold

Dongfeng Zhang[a], Yun Lin[b], Xi Chen[c], Wenting Zhao[a], Dongni Chen[b], Meng Gao[a], Qinglin Wang[b], Bin Wang[c], Haihong Huang[a,*], Yongjun Lu[b,*], Yu Lu[c,*]

[a] State Key Laboratory of Bioactive Substances and Function of Natural Medicine, Beijing Key Laboratory of Active Substance Discovery and Druggability Evaluation, Institute of Materia Medica, Peking Union Medical College and Chinese Academy of Medical Sciences, 1 Xian Nong Tan Street, Beijing 100050, China
[b] School of Life Sciences, Sun Yat-sen University, 135 West Xingang Road, Guangzhou, Guangdong 510275, China
[c] Beijing Key Laboratory of Drug Resistance Tuberculosis Research, Department of Pharmacology, Beijing Tuberculosis and Thoracic Tumor Research Institute, Beijing Chest Hospital, Capital Medical University, 97 Ma Chang Street, Beijing 101149, China

ARTICLE INFO

Keywords:
Tuberculosis
MptpB inhibitor
Virtual screening
Docking
Pharmacophore
Thiobarbiturate scaffold

ABSTRACT

Mycobacterium tuberculosis (*Mtb*) protein tyrosine phosphatase B (MptpB) is an important virulence factor for *Mtb* that contributes to survival of the bacteria in macrophages. The absence of a human ortholog makes MptpB an attractive target for new therapeutics to treat tuberculosis. MptpB inhibitors could be an effective treatment to overcome emerging TB drug resistance. Adopting a structure-based virtual screening strategy, we successfully identified thiobarbiturate-based drug-like MptpB inhibitor **15** with an IC_{50} of 22.4 μM, and as a non-competitive inhibitor with a K_i of 24.7 μM. Importantly, not only did it exhibit moderate cell membrane permeability, compound **15** also displayed potent inhibition of intracellular TB growth in the macrophage, making it an excellent lead compound for anti-TB drug discovery. To the best of our knowledge, this novel thiobarbiturate is the first class of MptpB inhibitor reported so far that leveraged docking- and pharmacophore-based virtual screening approaches. The results of preliminary structure-activity relationship demonstrated that compound **15** identified herein was not a singleton and may inspire the design of novel selective and drug-like MptpB inhibitors.

1. Introduction

With an estimated 1.3 million of tuberculosis deaths and an additional 374,000 deaths among HIV-positive people in 2016, tuberculosis is the ninth leading cause of death worldwide, and the leading cause of death as a single infectious disease [1]. In 2017, the World Health Organization reaffirmed commitment to end the TB epidemic by 2030 as envisaged in the Sustainable Development Goals (SDGs) [2]. However, the situation has recently become more serious with the development of multidrug-resistant tuberculosis (MDR-TB), extensively drug-resistant (XDR-TB) and totally drug-resistant tuberculosis (TDR-TB). Latent tuberculosis infection (LTBI) develops into active TB under certain conditions such as immunodeficiency. The aforementioned situations result in huge difficulties for treatment and control of TB [3]. Traditional anti-tubercular drugs target cell wall synthesis or inhibit bacterial growth, inevitably, which result in the selection of mutant strains that may develop drug resistance [4]. An alternative approach to the use of antibiotics is to block the action of virulence factors, thereby compromising the establishment of the infection and survival of the pathogen in the host [4]. Targeting secreted virulence factors could offer different advantages to circumvent the drug resistance problem [4]. Protein tyrosine phosphatases (PTPs) are often exploited and subverted by pathogenic bacteria to cause human diseases. *Mycobacterium tuberculosis* protein tyrosine phosphatase B (MptpB) is a crucial virulence factor that is secreted by the bacterium into the cytoplasm of macrophages, where it mediates mycobacterial survival and persistence in the host [5,6]. MptpB is an attractive and druggable anti-TB target due to very low sequence similarity to human phosphatases and the presence of a large hydrophobic active site [4,7]. However, there are two major challenges in PTP inhibitor development: specificity and cell permeability, due to conserved and highly positively charged active sites [8,9]. Large efforts have been invested on the improvement of

* Corresponding authors.
E-mail addresses: joyce@imm.ac.cn (H. Huang), luyj@mail.sysu.edu.cn (Y. Lu), luyu4876@hotmail.com (Y. Lu).

https://doi.org/10.1016/j.bioorg.2018.12.038
Received 25 September 2018; Received in revised form 23 December 2018; Accepted 29 December 2018
Available online 31 December 2018
0045-2068/

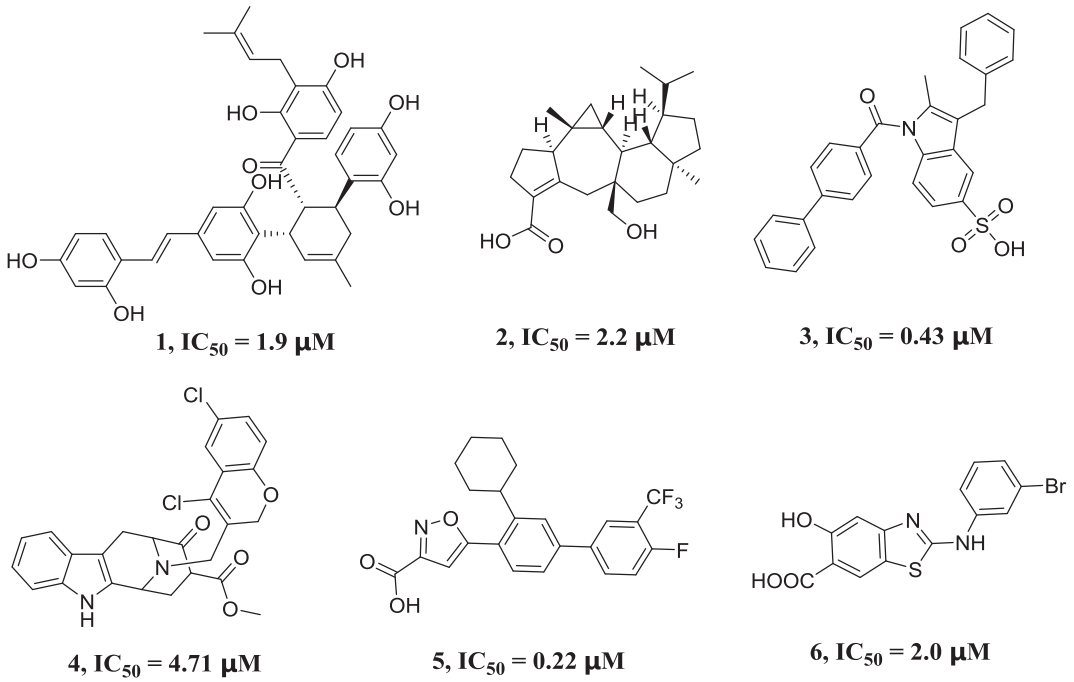

Fig. 1. Representative MptpB inhibitors.

selectivity and bioavailability of MptpB inhibitors, and significant progress has been made. Many potent inhibitors of MptpB, including those derived from natural products [10–12], via a biology-oriented synthesis approach using natural product scaffolds [13,14], or through rational design such as diversity-oriented synthesis and fragment-based strategy [8,15], etc., have been identified (Fig. 1). Although a handful of MptpB inhibitors have been reported [16], they often have complex structures, high molecular weight, or at least one acidic group, such as carboxylic acid [17–19] or sulfonic acid [14]. As such, these inhibitors are typically associated with poor cellular permeability and less druggability [20]. Inspired by the high-resolution co-crystal structure of MptpB with its inhibitor oxalylamino-methylene-thiophene sulfonamide (OMTS) reported by Tom Alber and coworkers [21], herein, we propose for the first time the docking- and pharmacophore-based virtual screening strategy to discover promising hits of MptpB inhibitors with novel and diverse structures, and more importantly drug-like properties.

Employing the structure-based virtual screening approach, a non-competitive MptpB inhibitor compound **15** with novel thiobarbiturate scaffold was successfully identified with IC_{50} of 22.4 μM. Importantly, compound **15** exhibited not only drug-likeness but also potent inhibition of intracellular TB growth in the macrophage. The outcome of our findings can shed more light on the search for novel and promising drug-like MptpB inhibitors as anti-TB agents.

2. Results and discussion

2.1. Virtual screening procedure

Virtual screening provides a unique opportunity to tap into unexplored chemical space in order to identify hit molecules as starting points for medicinal chemistry. Our strategy consists of docking- and pharmacophore-based virtual screening procedure to overcome their limitations [22]. In order to identify novel scaffolds in suitable molecular size and shape for the target active site, docking was performed prior to the pharmacophore-based approach. Firstly, the ZINC database containing more than 300,000 commercially available compounds was filtered by using Lipinski and Veber rules (Fig. 2) [23,24]. Secondly, the remaining 274,712 molecules were used in docking with Discovery Studio 2017R2. Next, the resulting database was filtered further by structure-based pharmacophore to afford 1,820 compounds. Lastly, duplicated structures or known inhibitors were removed. The resulting subset was inspected visually, and 20 compounds were purchased for further activity evaluation.

2.2. Docking-based virtual screening

The crystal structure of MptpB in a complex with its inhibitor OMTS (PDB code: 2OZ5) was used for docking studies [21]. The enzyme was obtained following a protocol in Discovery Studio 2017R2, by performing tasks such as adding missing atoms, modeling missing loop regions, deleting alternate conformations (disorder), removing waters, etc. The docking program (LigandFit) was evaluated by comparing the best docking pose obtained from the crystallized inhibitor OMTS (Fig. 3A) with its bound conformation. The results showed that the compound exhibited similar interactions to those of the original crystal structure with a root mean square deviation (RMSD) of 0.22 Å (Fig. 3B), indicating that the docking procedure was reliable.

Next, we evaluated seven scoring functions (LigScore1, LigScore2, Jain, -PLP1, -PLP2, -PMF and Dock_Score) by docking a set of MptpB inhibitors and inactive molecules into the active site using the LigandFit protocol. The results indicated that Dock_Score was better than the other scoring functions for distinguishing active from inactive compounds since all of active compounds could be picked up when Dock_Score > 90. The LigandFit was subsequently used to dock the compound library from the commercial ZINC database into the binding site. The resulting 28,362 compounds with Dock_Score > 90 were subjected to pharmacophore-based virtual screening.

2.3. Pharmacophore-based virtual screening

The Receptor-Ligand Pharmacophore Generation (RLPG) protocol in Discovery Studio 2017R2 was used to generate pharmacophore model based on receptor-ligand complex of the MptpB crystal structure (PDB code: 2OZ5). A set of well-known inhibitors and inactive molecules was prepared as a decoy set to validate the generated pharmacophore mode. The receiver operating characteristic curve (ROC) was 0.810, which suggested that a reliable pharmacophore model has been

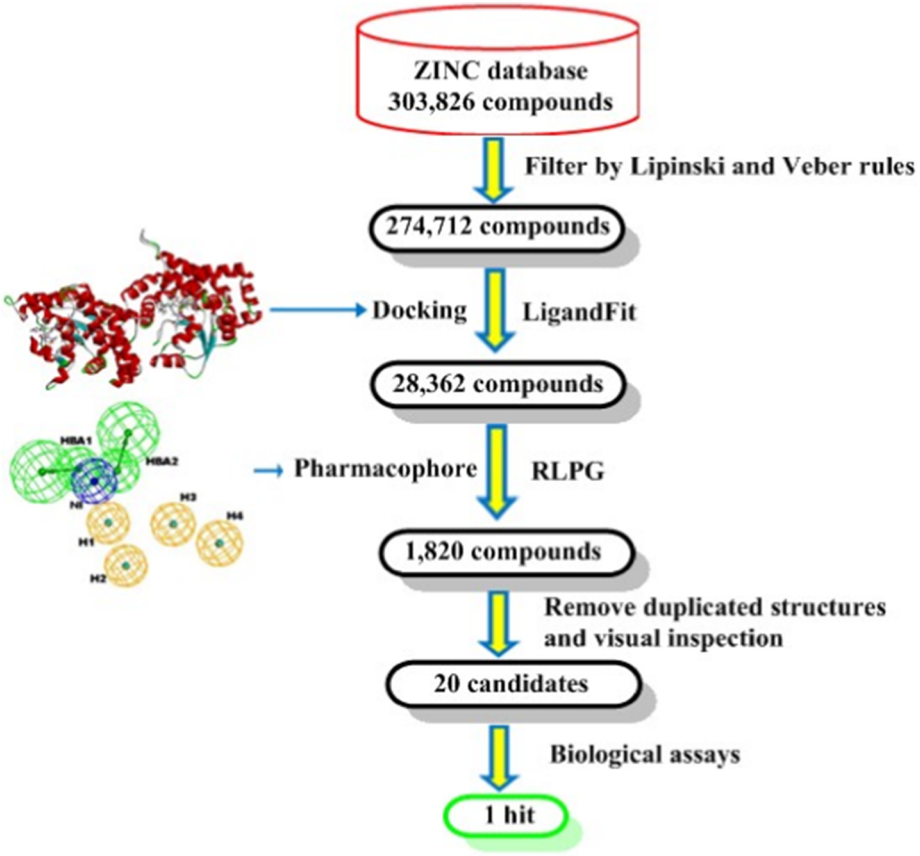

Fig. 2. Flowchart of the virtual screening procedures.

developed. The optimal pharmacophore model contained one negative ionizable group (NI), two hydrogen bond acceptors (HBA), and four hydrophobic groups (H) (Fig. 4).

Subsequently, the pharmacophore model was used to screen 28,362 molecules. A total of 1,820 small molecules that best fit the pharmacophore model were obtained. To further narrow down the compound list, firstly, the duplicated structures and compounds with already known scaffolds were removed. Then the final short list of hit compounds was generated based on visual inspection, with the selection criteria as following: (1) the relatively simpler structures will be selected among molecules of the same scaffold; (2) molecules of scaffold diversity will be selected; and (3) molecules containing at least one hydrogen bond acceptor pharmacophore feature will be selected, because hydrogen bond is very important interaction between ligand and receptor. At last, 20 candidates including 5 compounds containing carboxyl group were selected and purchased for biological evaluation (Table 1).

2.4. Hit identification

The selected candidates (20 compounds from more than 300,000 compounds) were experimentally screened against MptpB at 50 μM, and Na_3VO_4 was used as a positive control (Fig. 5). Five compounds showed > 20% inhibition at 50 μM concentration, and the IC_{50} value of the most potent compound **15** with the thiobarbiturate scaffold was further investigated (Table 2). To our delight, compound **15** displayed a moderate inhibitory activity with an IC_{50} value of 22.4 ± 2.5 μM.

To further investigate the inhibitory mode, we assessed the inhibition kinetics for MptpB at various concentrations of *p*-nitrophenyl phosphate (*p*NPP) and compound **15**. Compound **15** behaved as a non-competitive inhibitor of MptpB (Fig. 6) with a K_i constant of 24.7 ± 0.8 μM, a different inhibitory mode compared with OMTS [21] which is a competitive inhibitor. Further docking study was performed between MptpB and compound **15** as well as *p*-nitrophenyl phosphate (*p*NPP) to compare their binding modes. For *p*NPP, the phosphate group

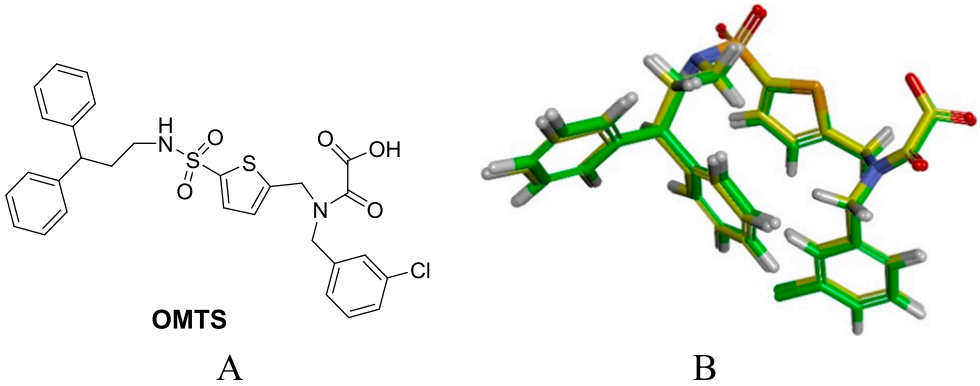

Fig. 3. The structure of OMTS (A) and overlays of crystallized OMTS with the docked poses (B) from LigandFit (RMSD 0.22 Å); X-ray structure: green; docked structure: yellow.

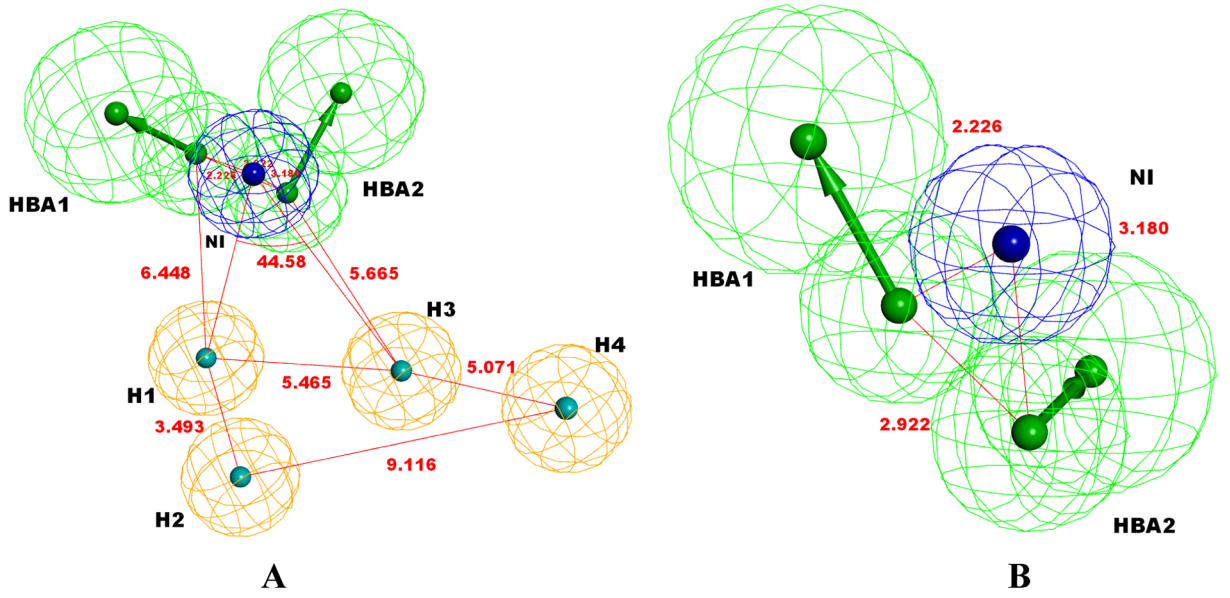

Fig. 4. The structure-based pharmacophore model of MptpB. (A) Features of the pharmacophore model; (B) Enlarged features of the pharmacophore model. The pharmacophore color: green for hydrogen bond acceptor, blue for negative ionizable group, orange for hydrophobic group.

was completely buried in the active site of MptpB, forming five hydrogen bonds with key residues (Phe161, Ala162, Gly163 and Asp165), which was consistent with OMTS (Fig. 7). For compound **15**, although it located in the same pocket of MptpB, different residues (Tyr125, Glu129, and Arg136) were found to form hydrogen bonds (Fig. 7). Moreover, there was almost no overlapping between the thiobarbiturate group of compound **15** and *p*NPP (Fig. 7). Above all, we attributed the non-competitive inhibitory mechanism of compound **15** to its specific binding pattern caused by the thiobarbiturate group, which was the key pharmacophore of this class of compound.

Based on the inhibitory mode of compound **15**, the precise ligand-receptor model was generated by the CDOCKER protocol in Discovery Studio 2017R2 (Fig. 8). The result displayed that there were three hydrogen bond interactions presented by CDOCKER. The hydrogen bonds were observed between the carbonyl oxygen of compound **15** and the hydroxyl hydrogen of Tyr125, the amide hydrogen of compound **15** and the carbonyl oxygen of Glu129, and the sulfur of compound **15** and the amino hydrogen of Arg136. Meanwhile, the middle phenyl ring of compound **15** formed ion-π interactions with residues Arg166 and Glu60. The chlorophenyl moiety of compound **15** had no obvious interactions with the active site of MptpB, which may be the key point for further structural modification to enhance the activity.

Compound **15** was evaluated for its antimycobacterial activities against *Mtb* $H_{37}Rv$ using the microplate alamar blue assay (MABA) and further tested for its cytotoxicity against mammalian cell line (Vero cells) [25]. As shown in Table 2, compound **15** exhibited low cytotoxicity with $IC_{50} > 64\ \mu g/mL$. As MptpB is a secreted virulence factor that regulates host antibacterial responses rather than *Mtb* physiology, it was not surprising that compound **15** was inactive in standard MIC assays. To our delight, compound **15** has not only suitable H-bond donors and acceptors but also satisfied TPSA value with 67.4 $Å^2$ [26]. It was noted that compound **15** displayed acceptable lipophilicity with Clog*P* 4.61, providing a good opportunity to enter macrophages.

2.5. Preliminary druggability evaluation of compound 15

Combination therapies of current anti-TB agents with MptpB inhibitors probably is the key to the clearance of infection and reduction of persistence of TB [4]. To understand the possibility of compound **15** as one component in the combination regimen, more assessments of druggability were evaluated. As summarized in Table 3, compound **15** exhibited not only moderate cell membrane permeability which is consistent with its moderate Clog*P*, but also excellent metabolic stability in mouse liver microsome and human liver microsome. Moreover, compound **15** had no observable inhibitory activity against most of the major CYP isoforms, which indicated a low risk of drug-drug interactions of compound **15** in the potential combination regimens, which is a very important property for treatment of tuberculosis.

2.6. Cellular activity of MptpB inhibitor compound 15

Mtb is an intracellular pathogen whose primary target cells are macrophages. Given the good potency toward MptpB and favorable pharmacological properties of compound **15**, we proceeded to evaluate its cellular efficacy J774A.1 macrophages infected with *Mtb* $H_{37}Rv$ (Fig. 9). In the absence of the inhibitors (control), bacterial burden was about 4.33 (log_{10}CFU) after 72 h of infection. When macrophages were treated with 5 μg/mL of compound **15**, intracellular mycobacterial growth was substantially reduced by a log_{10}CFU of 1.02, compared with the control. Compound **15** exhibited equivalent potent anti-tuberculosis activity in macrophages compared to rifampin (RFP) at 5 μg/mL concentration. This study provided further evidence to support the concept that specific inhibitors of MptpB may be effective anti-TB agents. Compound **15** with novel thiobarbiturate scaffold could be as a valuable lead for further development of anti-TB drug candidate with more potency and druggability targeting MptpB.

2.7. Preliminary structure-activity relationship of compound 15

Based on the promising biological results, we explored the preliminary structure-activity relationship (SAR) of compound **15**. As shown in Table 4, keeping the potential key pharmacophore thiobarbiturate group, removal of 4-chlorophenyl of compound **15** led to a significant loss of MptpB inhibitory activity (**27**). When R_1 was chlorine, compound **28** showed comparable potency to that of **15**. Replacement of the 4-chlorophenyl with larger aromatic groups (**29–31**) led to equivalent of potency, suggesting that it could accommodate bulky substitution. There is no significant effect on MptpB inhibitory activity with thiobarbiturate group at the 3-position of the middle phenyl core (**32**), however, thiobarbiturate group at the 4-position led to significant loss of potency (**33**). The results indicated that, rather than a singleton, compound **15** was an example of the active

Table 1
The chemical structures of selected candidates.

Compd.	Specs ID-number	Structure
7	AN-655/15449006	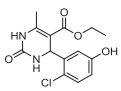
8	AG-205/10474008	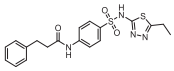
9	AG-205/40045468	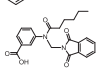
10	AK-968/40734886	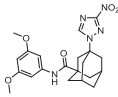
11	AG-690/40751841	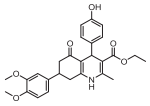
12	AQ-360/42570735	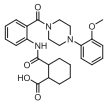
13	AQ-360/42570575	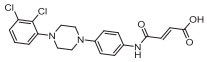
14	AJ-292/12941015	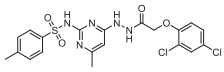
15	AM-879/12214034	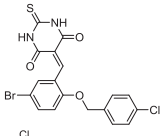
16	AM-879/12976006	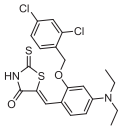
17	AQ-390/42425597	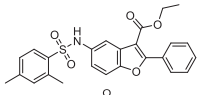
18	AQ-390/40882272	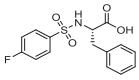
19	AQ-390/42698353	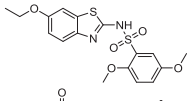
20	AQ-750/42210756	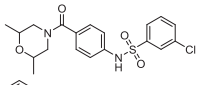
21	AS-662/43412909	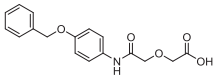
22	AN-465/13672320	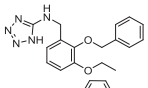
23	AP-263/43418898	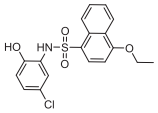
24	AO-022/41785017	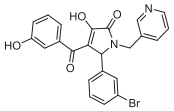
25	AO-022/42287969	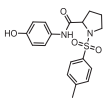

Table 1 (*continued*)

Compd.	Specs ID-number	Structure
26	AO-022/42398624	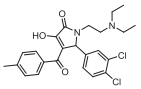

chemotypes that could be explored further to develop more potent inhibitors.

The synthetic route was outlined in Scheme 1. 5-Bromo-2-methoxybenzaldehyde (**27a**) was reacted with 2-thiobarbituric acid in conc. HCl at 70 °C to afford the target compound **27** (Scheme 1A). Benzaldehydes (**28-29a**, **32-33a**) were firstly alkylated with different compounds (**28-31b**) in DMF at 120 °C to yield the intermediates **28-33c**, which were subsequently reacted with 2-thiobarbituric acid to furnish the target compounds **28–33** (Scheme 1B and 1C).

3. Experimental protocols

3.1. Virtual screening methods

3.1.1. Protein and database preparation

The X-ray crystal structure of MptpB in a complex with inhibitor OMTS in the higher resolution of 2 Å (PDB code: 2OZ5) was used for virtual screening [21]. The protein structure was firstly prepared by adding the hydrogen atoms, inserting the missing loop regions, removing the waters molecules, adding missing atoms and deleting alternate conformations (disorder) using the Prepare Protein protocol in Discovery Studio 2017R2. The chemical library for virtual screening was obtained from the ZINC database containing more than 300,000 commercially available compounds. The database was firstly filtered by using Lipinski's rule of five and Veber rule by Filter tool in Discovery Studio 2017R2, and then was prepared by Prepare Ligands protocol, performing tasks such as removing duplicates, enumerating isomers and tautomers, and generating 3D conformations. The resulted ligands database was split to 20 subsets for docking procedure.

3.1.2. Molecular docking

Molecular docking studies were performed using LigandFit option of receptor-ligand interactions protocol section available in Discovery Studio 2017R2. The protein molecule thus prepared was defined as the receptor. Two molecules of OMTS bound one molecule of MptpB in the crystal structure, we selected proximal OMTS to define binding site because of this molecule had extensive interactions with the catalytic site in the crystal structure that contribute to binding affinity and specificity [21]. Before virtual screening, we validated the accuracy of the screening model and protocol by reproducing the binding pose of the OMTS in the crystal structure, through which we found that the best docked pose obtained a minimum RMSD as 0.22 Å against the original binding pose in the crystal structure (Fig. 3B), which proved the reliability of the screening model and method used in this study. The conformational search of the ligand poses was performed by the Monte Carlo trial method. Five poses were saved for each ligand after docking and only one pose was retained with the highest Dock_Score, compounds with Dock_Score more than 90 were retained within each subset for further pharmacophore-based virtual screening.

3.1.3. Pharmacophore modeling

The prepared protein (PDB code: 2OZ5) was used for generating a pharmacophore model using the Receptor-Ligand Pharmacophore Generation (RLPG) protocol in Discovery Studio 2017R2. The proximal OMTS was used as input ligand to generate pharmacophore model, and the obtained pharmacophore models were validated by using a set of well-known inhibitors and inactive molecules as a decoy set. The

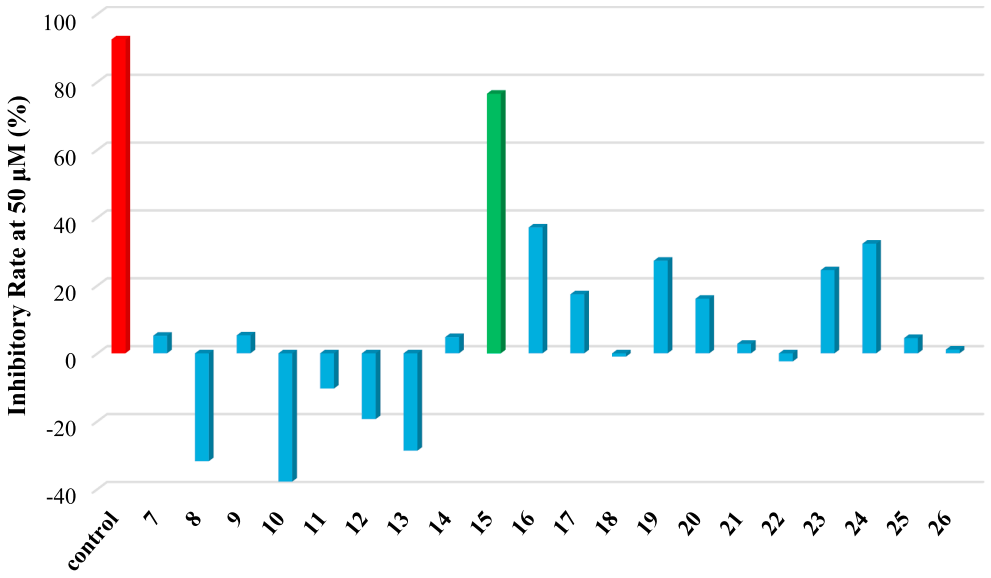

Fig. 5. Inhibition of MptpB activity of the selected candidates.

pharmacophore model with receiver operating characteristic curve (ROC) 0.810 was selected to screen the ligand molecules retained by docking, and the ligands with FitValue more than 3 were selected as the final compounds library to choose candidates for biological assay.

*3.1.4. Binding mode and molecular interactions analysis of compound **15***

To determine the potential binding mode of compound **15**, we performed a refinement step using CDOCKER. First, compound **15** was minimized by Full Minimization tool using CHARMm forcefield. Then, compound **15** was docked to the binding site. This procedure consisted in a simulated annealing refinement (2000 steps at 700 K, 5000 steps at 300 K) followed by a final full force field minimization using CHARMm. The top 10 poses were retained with the favorable binding mode, and one of them has been selected with the highest -CDOCKER_ENERGY.

3.2. Inhibition assays for MptpB

The phosphatase activity of MptpB was assayed in triplicates in 96-well microplates in reaction buffer (50 mM Tris/100 mM NaCl, pH 7.0) using *p*-nitrophenyl phosphate (*p*NPP) (Aladdin) as a substrate. To screen compounds for MptpB inhibition, the assay was conducted in a 200 μL reaction system containing 1.5 μg MptpB protein and 50 μM tested compounds. The reaction mixture was incubated for 10 min at room temperature, followed by the addition of *p*NPP to a final concentration of 1.3 mM (the K_m value). The absorbance at 405 nm was measured for 5 min, at 37 °C in the spectrophotometer Infinite 200 PRO (TECAN). Control reactions without MptpB were included to account for the spontaneous hydrolysis of *p*NPP.

IC_{50} of compound with more than 50% of inhibitory activity against MptpB was determined at different concentrations using two-fold serial dilution (1.5625–100 μM). The data was calculated by fitting the inhibition percentage and inhibitor concentrations with Origin 9. To determine the type of inhibition, different inhibitor concentrations (0 μM, 20 μM and 60 μM) and different concentrations of *p*NPP (0.05 mM, 0.1 mM, 0.2 mM, 0.4 mM, 0.8 mM, 1.6 mM, and 3.2 mM) were performed as explained above. The type of inhibition was determined by fitting data to Lineweaver-Burk plot by double reciprocal of inhibitor concentration versus velocity. All assays were performed in triplicate in at least three independent experiments.

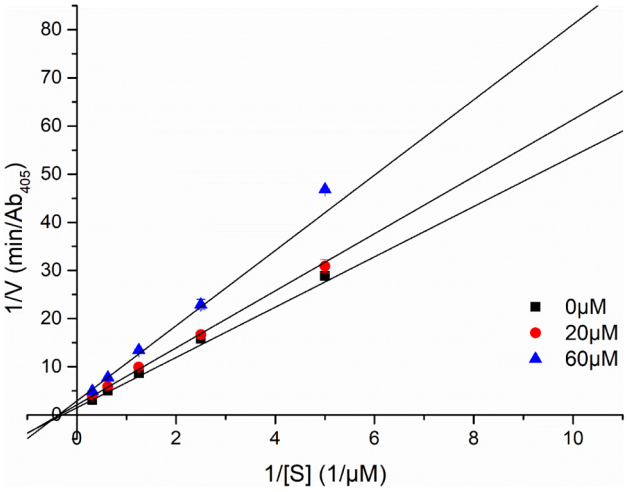

Fig. 6. Lineweaver-Burk plot for compound **15** on MptpB inhibition. Compound **15** behaved as a non-competitive inhibitor.

3.3. Minimum inhibitory concentration (MIC) and cytotoxicity assay

Compound **15** was evaluated for its antimycobacterial activities against *Mtb* $H_{37}Rv$ using the microplate alamar blue assay (MABA). The minimum inhibitory concentration (MIC) was defined as the lowest concentration effecting a reduction in fluorescence of ≥ 90% relative to the mean of replicate bacterium-only controls. This compound was

Table 2
IC_{50} and K_i values on MptpB, MIC, cytotoxicity and physicochemical properties of compound **15**.

IC_{50} (μM)[a]	K_i (μM)[a]	MIC (μg/mL)	Cytotoxicity (μg/mL)	Clog*P*	H-bond donors	H-bond acceptors	TPSA[b] (Å^2)
22.4 ± 2.5	24.7 ± 0.8	> 32	> 64	4.61	2	4	67.4

[a] IC_{50} = mean ± SD (n = 3), K_i = mean ± SD (n = 3).
[b] TPSA: Topological Polar Surface Area, calculated by ChemDraw 2012.

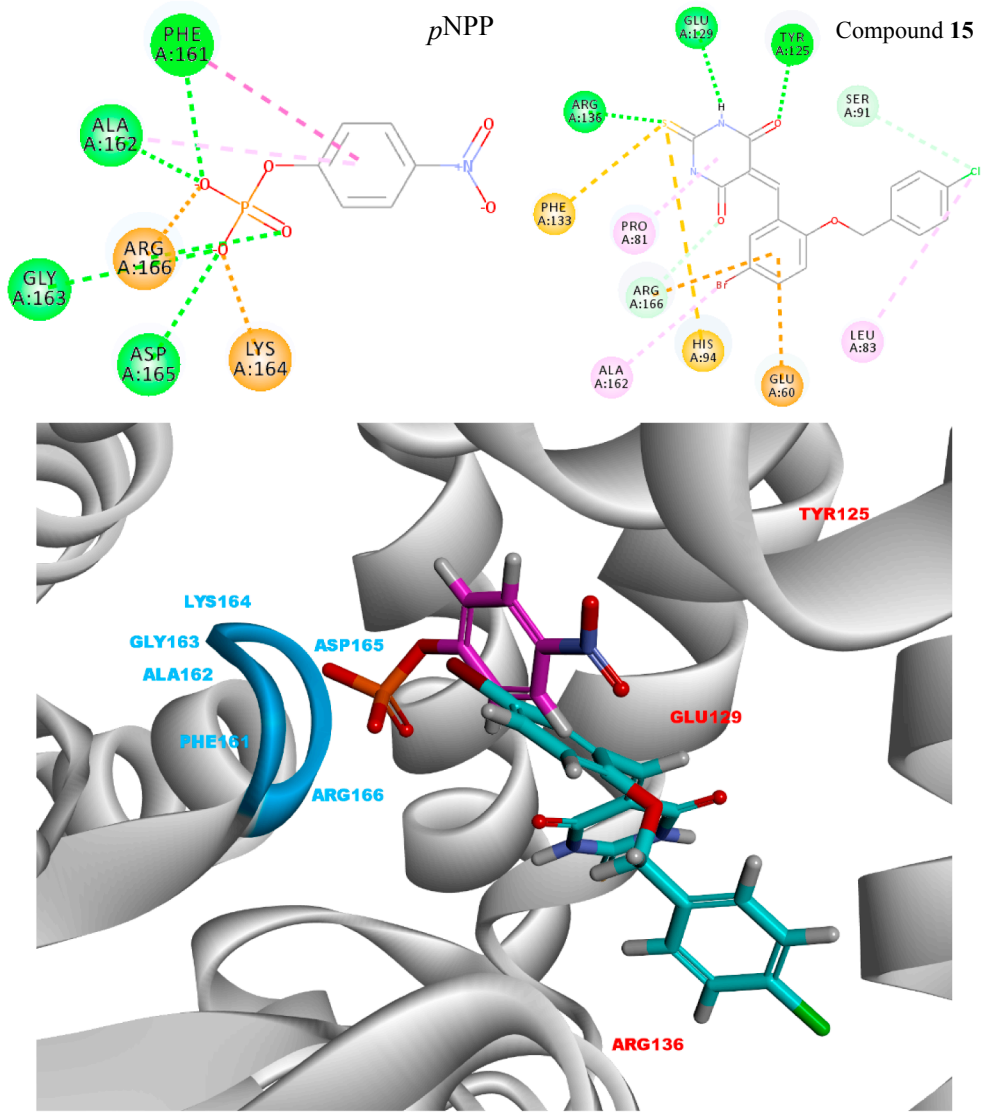

Fig. 7. Binding mode and interaction pattern of *p*-nitrophenyl phosphate (*p*NPP) and compound **15** with MptpB. Compound **15** is shown as cyan, *p*NPP is shown as pink.

further tested for its cytotoxicity against mammalian cell line (Vero cells) as measured by the concentration required for inhibiting 50% cell growth (IC_{50}) as compared to the no-treatment control [25].

3.4. Liver microsomal stability assay

Compound **15** (1 μM, 2.5 μL) was incubated with mouse or human liver microsomes (1 mg/mL) in phosphate buffer (50 mM, pH 7.4, 197.5 μL). The medium containing compound was incubated at 37°C for 5 min, and then 50 μL NADPH working solution (1 mM) was added to initial the reaction. At each time point (0 and 30 min), remove 30 μL of the reaction mixture for future analysis. All reactions were terminated by adding 300 μL Methanol/ACN (1:1, v/v). The remaining fraction of compound was quantified by LC-MS/MS assay. Midazolam, Dextromethorphan, Declofenac, Omeprazole, and Phenacetin (5 μM) are used as controls.

3.5. Caco-2 permeability assay

The cells were seeded onto filter transwell inserts at a density of ~32,000 cells/well in DMEM cell culture mediumin and formed a confluent monolayer after 22 days culture. On day 22, the compound **15** (3 μM) was added into the apical side of the membrane and the concentration of the compound across Caco-2 cell monolayer was quantified by LC-MS/MS after 90 min incubation at 37 °C. Transepithelial electrical resistance (TEER) should be determined before as well as after transport experiments and should be greater than 600 Ω/cm^2. The apparent permeability coefficient (Papp) for the compound is calculated from the following equation:

$$\text{Papp} = (\text{Conc.}_{\text{receiver,90 min}} \times \text{Volume}_{\text{receiver}}) / (\text{Time} \times \text{Membrane Area} \times \text{Conc.}_{\text{donor,0 min}})$$

3.6. Cytochromes P450 (CYP) inhibition assay

CYP inhibition potential of compound **15** toward the major human isoforms CYP1A2, CYP2C9, CYP2C19, CYP2D6 and CYP3A4 was determined using human liver microsome. The incubation mixtures (0.2 mL) contained Tris-HCl buffer (0.05 M, pH 7.4), human liver microsome (0.2 mg/mL), the test compound, NADPH-regenerating system (10 mM β-NADP, 100 mM 6-G-P and 10 U/mL 6-G-P-DH), and a CYP450 sensitive substrate. A reference inhibitor for each enzyme (β-naphthoflavone for CYP1A2, sulfaphenazole for CYP2C9,

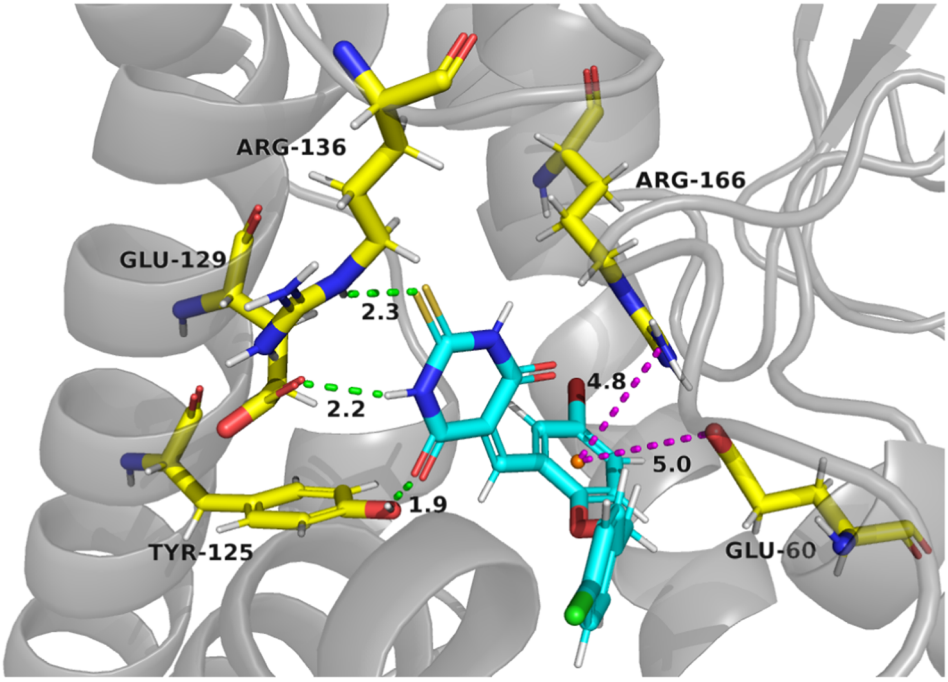

Fig. 8. Predicted binding mode and interaction pattern of compound **15** with MptpB obtained from CDOCKER. Compound **15** is shown as cyan, and the hydrogen bonds are indicated as green lines; anion–π and cation–π interactions are indicated as purple lines.

Table 3
Preliminary druggability properties of compound **15**.

Caco-2 Papp ($\times 10^{-6}$ cm/s)		1.91			
Liver microsome stability		Stability[a]	Substrate remaining (%)[b]	$T_{1/2}$ (min)	Cl_{int} (μL/min/mg protein)
	Mouse	Stable	112	> 500	< 1.39
	Human	Stable	111	> 500	< 1.39
CYP inhibition IC_{50} (μM)	1A2	2C9	2C19	2D6	3A4
	4.97	21.1	> 50	> 50	> 50

[a] Stability was determined without the NADPH cofactor.
[b] Substrate concentrations were determined in incubations with NADPH after 30 min.

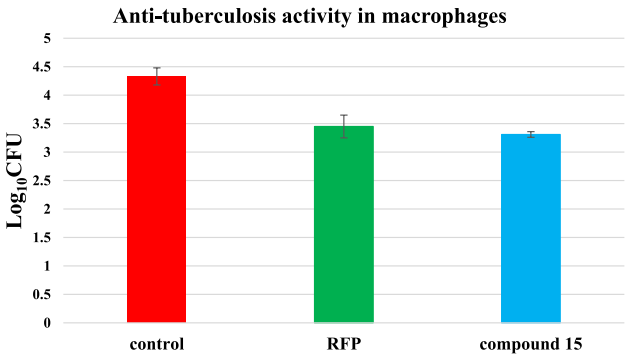

Fig. 9. Treatment with compound **15** reduced *Mtb* survival in infected macrophages. Concentrations of RFP and compound **15** were 5 μg/mL.

tranylcypromine for CYP2C19, quinidine for CYP2D6 and ketoconazole for CYP3A4) was used as a positive control. After addition the test compound, the samples were then incubated at 37 °C for 20 min with shaking. All reactions were terminated by adding acetonitrile (0.3 mL). Probe substrate-derived metabolites were quantified by LC-MS/MS. IC_{50} was calculated using Graph Pad Prism.

3.7. Anti-tuberculosis activity in macrophages

J774A.1 cells were incubated at 37 °C in 5% CO_2 in a culture medium consisting of DMEM medium supplemented with 10% fetal bovine serum in 75 cm^2 culture dishes until cells cover 80% area of culture dishes. After treatment with 0.25% pancreatic enzymes, the cells were resuspended with 10 mL DMEM medium supplemented with 10% fetal bovine serum, then transferred to 10 mL centrifuge tube. Centrifuge for 5 min at 1000 rpm to collect cell deposition. Adjusted the cell concentration to 8×10^5 cells/mL with DMEM medium containing 10% fetal bovine serum. J774A.1 cells were seeded in 48-well plates at 4.0×10^5 cells/well and incubated for 16 h at 37 °C in 5% CO_2 in DMEM medium supplemented with 10% fetal bovine serum. The *Mtb* H_{37}Rv strains were grown at 37 °C to mid-log phase in Middlebrook 7H9 broth (BD Bioscience) supplemented with 10% OADC, and 0.05% Tween 80. Bacteria were harvested, filtered with 80 μm filter membrane to remove the bacterial clumps. Recorded the Optical Density at 570 nm (OD570) using the multimode reader (OD570 0.1 = 10^8 CFU/mL). Adherent J774A.1 cells were infected with *Mtb* H_{37}Rv strain at a multiplicity of infection (MOI) of 5 for 4 h. After discarding the culture medium, the cells were washed twice with 1 × PBS buffer to remove extracellular bacteria. The cells were cultured further in 1 mL DMEM medium containing 10% FCS for 3 days in the presence or absence of compounds. The final concentration of compound **15** was 5 μg/mL, and rifampin (RFP) as the positive control was 5 μg/mL. Following 3 days incubation at 37 °C, culture medium was discarded. Cells were lysed in 200 μL 0.1% SDS cell lysis buffer for 5 min, and neutralized by 800 μL culture medium. The number of viable bacteria in each well was enumerated by plating the cell lysate on Middlebrook 7H11 agar plates and colony counting after incubation for 21 days. All assays were performed in triplicate in at least three separate experiments.

3.8. Synthesis of compounds *27–33*

3.8.1. General methods

All the starting materials were obtained from commercial suppliers and were used without further purification unless stated otherwise. Reactions were monitored by TLC (silica gel GF254). ^{1}H NMR spectra

Table 4
Preliminary structure-activity relationship (SAR) of compound **15.**

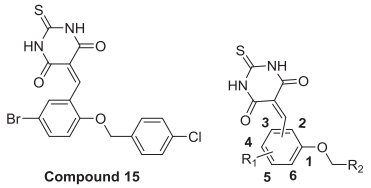

Compd.	Structure	MptpB Inhibitory Activity % (50 μM)	IC_{50} (μM)
27	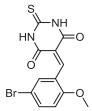	−7.7	–
28	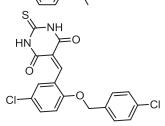	67.8	17.4
29	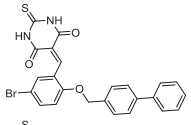	53.5	16.2
30	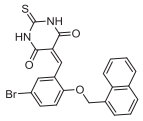	69.5	36.3
31	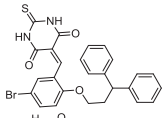	40.9	–
32	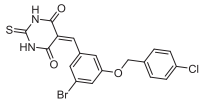	51.6	32.1
33	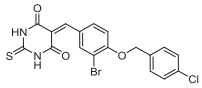	27.2	–
Control		93.4	

were recorded on a Varian 400 NMR or 500 NMR spectrometer using DMSO-d_6 as a solvent and tetramethylsilane (TMS) as an internal standard. Chemical shift (δ) are reported in parts per million (ppm) and coupling constants (*J*) are reported in Hertz (Hz). Data are represented as follows: chemical shift, multiplicity (br = broad, s = singlet, d = doublet, dd = double doublet, t = triplet, m = multiplet), coupling constants in Hertz (Hz), integration. All melting points were measured with a microscope melting point apparatus (MP-J3, Yanaco) and were uncorrected. High-resolution mass spectra were determined on ThermoExactive Orbitrap plus mass spectrometer.

*3.8.2. 5-(5-Bromo-2-methoxybenzylidene)-2-thiobarbituric acid (**27**)*

A mixture of 5-bromo-2-methoxybenzaldehyde **27a** (0.65 g, 3 mmol) and 2-thiobarbituric acid (0.43 g, 3 mmol) in conc. HCl (10 mL) was heated at 70 °C for 3 h. The resulting precipitate was filtered off and then washed with hot H_2O to give the solid. The crude product was refluxed in MeOH (5 mL), after filtration, the precipitate was washed with MeOH and dried to give compound **27** as a yellow solid (0.82 g, 80%). MP: > 250 °C. ^{1}H NMR (500 MHz, DMSO-d_6) δ 12.47 (s, 1H), 12.33 (s, 1H), 8.35 (s, 1H), 8.20 (d, J = 1.5 Hz, 1H), 7.69 (dd, J = 9.0, 1.5 Hz, 1H), 7.10 (d, J = 9.0 Hz, 1H), 3.89 (s, 3H). HR-MS (ESI): *m/z* $[M-H]^-$ calcd for $C_{12}H_8BrN_2O_3S$: 338.9434; found: 338.9412.

*3.8.3. General procedure for the synthesis of compounds **28**–**33***

To a mixture of substituted salicylaldehyde analogues (3 mmol) and K_2CO_3 (6 mmol) in DMF (10 mL) was added compounds **28-31b** (3.3 mmol). The reaction mixture was stirred at 120 °C for 4 h. The mixture was cooled to room temperature. H_2O (30 mL) was added and the mixture was filtered to afford the intermediates **28-33c**, which were used in next step without purification. The target compounds were prepared by the procedure as described in compound **27**. Conc. HCl (10 mL) was the reaction solvent for the synthesis of compounds **28**, **29** and **33**. EtOH (20 mL) and conc. HCl (10 mL) were the reaction solvents for the synthesis of compounds **30**–**32**.

*3.8.3.1. 5-(5-Chloro-2-((4-chlorobenzyl)oxy)benzylidene)-2-thiobarbituric acid (**28**)*. Yellow solid (0.72 g, 59%). MP: 238–240 °C. ^{1}H NMR (400 MHz, DMSO-d_6) δ 12.44 (s, 1H), 12.31 (s, 1H), 8.40 (s, 1H), 8.07 (d, J = 2.8 Hz, 1H), 7.56 (dd, J = 8.8, 2.8 Hz, 1H), 7.47 (s, 4H), 7.21 (d, J = 9.2 Hz, 1H), 5.24 (s, 2H). HR-MS (ESI): *m/z* $[M-H]^-$ calcd for $C_{18}H_{11}Cl_2N_2O_3S$: 404.9862; found: 404.9835.

*3.8.3.2. 5-(2-([1,1′-Biphenyl]-4-ylmethoxy)-5-bromobenzylidene)-2-thiobarbituric acid (**29**)*. Yellow solid (0.38 g, 25%). MP: 220–222 °C. ^{1}H NMR (400 MHz, DMSO-d_6) δ 12.46 (s, 1H), 12.33 (s, 1H), 8.45 (s, 1H), 8.22 (d, J = 2.8 Hz, 1H), 7.72–7.67 (m, 4H), 7.54 (d, J = 8.4 Hz, 2H), 7.49–7.45 (m, 3H), 7.38 (t, J = 7.2 Hz, 1H), 7.22 (d, J = 9.2 Hz, 1H), 5.31 (s, 2H). HR-MS (ESI): *m/z* $[M-H]^-$ calcd for $C_{24}H_{16}BrN_2O_3S$: 491.0060; found: 491.0024.

*3.8.3.3. 5-(5-Bromo-2-(naphthalen-1-ylmethoxy)benzylidene)-2-thiobarbituric acid (**30**)*. Yellow solid (0.98 g, 70%). MP: 235–237 °C. ^{1}H NMR (400 MHz, DMSO-d_6) δ 12.38 (s, 1H), 12.28 (s, 1H), 8.36 (s, 1H), 8.19 (d, J = 2.8 Hz, 1H), 8.13–8.10 (m, 1H), 7.99–7.93 (m, 2H), 7.72–7.66 (m, 2H), 7.60–7.49 (m, 3H), 7.41 (d, J = 9.2 Hz, 1H), 5.71 (s, 2H). HR-MS (ESI): *m/z* $[M-H]^-$ calcd for $C_{22}H_{14}BrN_2O_3S$: 464.9903; found: 464.9862.

*3.8.3.4. 5-(5-Bromo-2-(3,3-diphenylpropoxy)benzylidene)-2-thiobarbituric acid (**31**)*. Yellow solid (0.46 g, 29%). MP: 210–212 °C. ^{1}H NMR (400 MHz, DMSO-d_6) δ 12.52 (s, 1H), 12.36 (s, 1H), 8.55 (s, 1H), 8.28 (d, J = 2.4 Hz, 1H), 7.59 (dd, J = 8.8, 2.4 Hz, 1H), 7.37–7.35 (m, 4H), 7.29–7.25 (m, 4H), 7.18–7.14 (m, 2H), 6.97 (d, J = 9.2 Hz, 1H), 4.27 (t, J = 8.0 Hz, 1H), 3.98 (t, J = 6.0 Hz, 2H), 2.55–2.53 (m, 2H). HR-MS (ESI): *m/z* $[M-H]^-$ calcd for $C_{26}H_{20}BrN_2O_3S$: 519.0372; found: 519.0331.

*3.8.3.5. 5-(3-Bromo-5-((4-chlorobenzyl)oxy)benzylidene)-2-thiobarbituric acid (**32**)*. Yellow solid (0.92 g, 68%). MP: > 250 °C. ^{1}H NMR (400 MHz, DMSO-d_6) δ 12.49 (s, 1H), 12.36 (s, 1H), 8.18 (s, 1H), 7.91 (s, 1H), 7.71 (s, 1H), 7.48 (brs, 4H), 7.41 (t, J = 2.0 Hz, 1H), 5.17 (s, 2H). HR-MS (ESI): *m/z* $[M-H]^-$ calcd for $C_{18}H_{11}BrClN_2O_3S$: 448.9357; found: 448.9322.

*3.8.3.6. 5-(3-Bromo-4-((4-chlorobenzyl)oxy)benzylidene)-2-thiobarbituric acid (**33**)*. Yellow solid (0.96 g, 71%). MP: > 250 °C. ^{1}H NMR (400 MHz, DMSO-d_6) δ 12.43 (s, 1H), 12.34 (s, 1H), 8.87 (d, J = 2.0 Hz, 1H), 8.24–8.22 (m, 2H), 7.54–7.48 (m, 4H), 7.32 (d, J = 8.8 Hz, 1H), 5.36 (s, 2H). HR-MS (ESI): *m/z* $[M-H]^-$ calcd for $C_{18}H_{11}BrClN_2O_3S$: 448.9357; found: 448.9324.

4. Conclusions

Regarding the importance of MptpB for mycobacteria survival in the host, inhibition of MptpB represents an effective approach for the treatment of TB. To address the common issues of selectivity and cell permeability of MptpB inhibitors, with the aid of the crystallographic structure of MptpB in complex with OMTS, we exploited the docking-based and pharmacophore-based virtual screening of a commercially

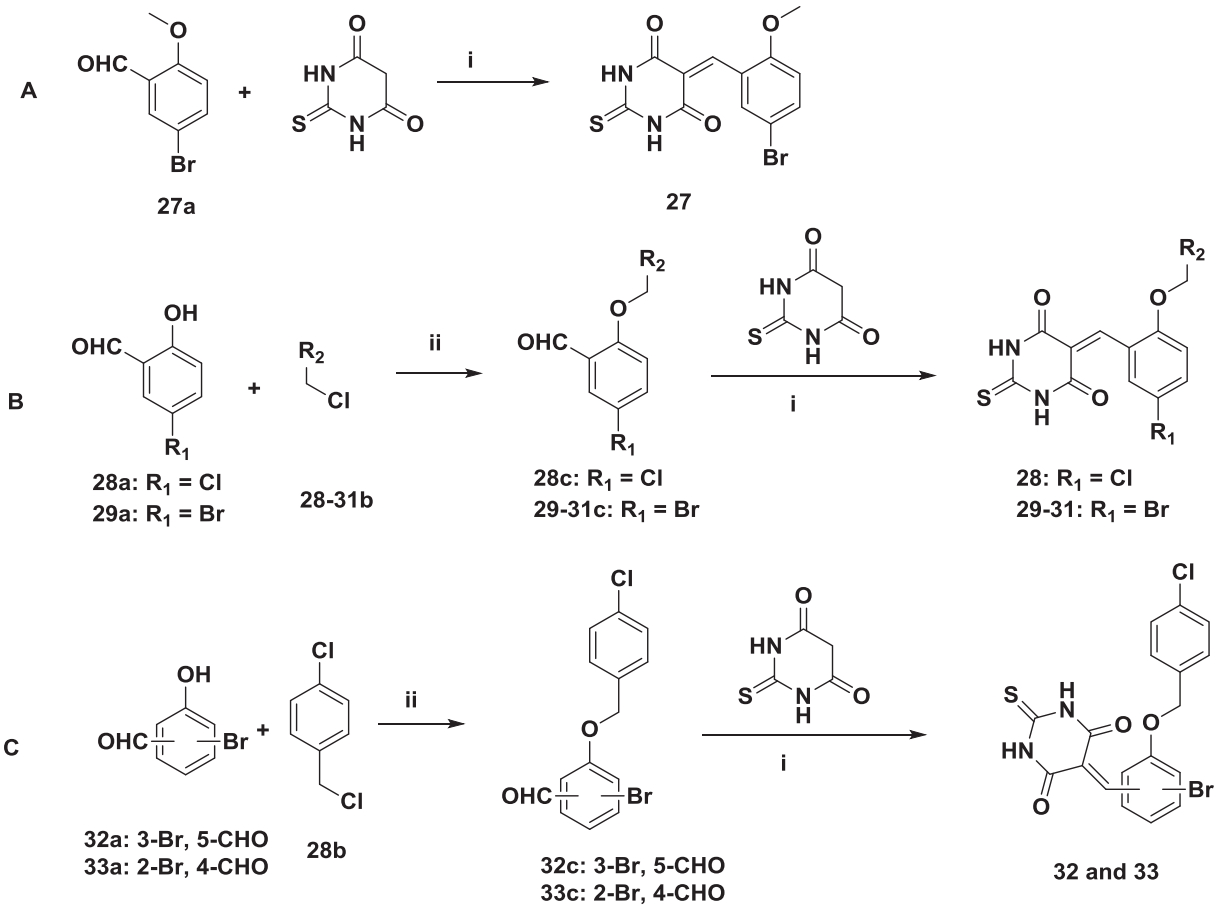

Scheme 1. Reagents and conditions: (i) HCl, 70 °C or HCl, EtOH, 70 °C; (ii) K_2CO_3, DMF, 120 °C.

available ZINC database combined with biological testing. Compound **15** was identified as a promising MptpB inhibitor with novel thiobarbiturate scaffold. Compound **15** displayed good inhibitory activity with IC_{50} of 22.4 μM as a non-competitive inhibitor of MptpB with a K_i constant of 24.7 μM. Importantly, compound **15** exhibited good druggability profiles including excellent liver microsome stability and low drug-drug interaction risk, especially acceptable cell membrane permeability, which makes it possible to kill *Mtb* in macrophages. Preliminary data from cell infection models demonstrated that compound **15** as a MptpB inhibitor can effectively reduce the mycobacterial load in infected macrophages. The small size of compound **15** opens opportunities for further elaborations to improve activity and druggability. In particular, the outcome of our findings offers a successful example of employing virtual screening as an effective approach to discover new chemotypes of MptpB inhibitors. The results of the preliminary structure-activity relationship (SAR) of compound **15** demonstrated that this hit was not a singleton. Further structural modification based on compound **15** will be performed to develop potent and specific MptpB inhibitors as anti-TB agents in due course.

Acknowledgements

We gratefully acknowledge financial support from the CAMS Innovation Fund for Medical Sciences (CIFMS) under Grant No. 2016-I2M-1-013.

Conflict of interest

The authors declare that there are no conflicts of interest.

References

[1] World Health Organization. Global tuberculosis report 2017, < http://www.who.int/tb/publications/global_report/en/ > .
[2] Moscow Declaration to End TB, First WHO Global Ministerial Conference Ending TB in The Sustainable Development Era: A Multisectoral Response, 16–17 November 2017, < http://www.who.int/tb/endtb-sdg-ministerial-conference/en/ > .
[3] S. Caño-Muñiz, R. Anthony, S. Niemann, J.C. Alffenaar, Clin. Microbiol. Rev. 31 (2018) e00060–17.
[4] A.P. Silva, L. Tabernero, Future Med. Chem. 2 (2010) 1325–1337.
[5] B. Zhou, Y. He, X. Zhang, J. Xu, Y. Luo, Y. Wang, S.G. Franzblau, Z. Yang, R.J. Chan, Y. Liu, J. Zheng, Z.Y. Zhang, Proc. Natl. Acad. Sci. USA 107 (2010) 4573–4578.
[6] R. He, L.F. Zeng, Y. He, L. Wu, A.M. Gunawan, Z.Y. Zhang, Chem. Commun. 49 (2013) 2064–2066.
[7] M.A. Ghattas, N. Raslan, A. Sadeq, M. Al Sorkhy, N. Atatreh, Drug Des. Devel. Ther. 10 (2016) 3197–3209.
[8] R. He, Y. Bai, Z.H. Yu, L. Wu, A.M. Gunawan, Z.Y. Zhang, MedChemComm. 5 (2014) 1496–1499.
[9] Z.Y. Zhang, Curr. Opin. Chem. Biol. 5 (2001) 416–423.
[10] D. Müller, A. Krick, S. Kehraus, C. Mehner, M. Hart, F.C. Küpper, K. Saxena, H. Prinz, H. Schwalbe, P. Janning, H. Waldmann, G.M. König, J. Med. Chem. 49 (2006) 4871–4878.
[11] X. Huang, H. Huang, H. Li, X. Sun, H. Huang, Y. Lu, Y. Lin, Y. Long, Z. She, Org. Lett. 15 (2013) 721–723.
[12] A. Mascarello, M. Mori, L.D. Chiaradia-Delatorre, A.C. Menegatti, F. Delle Monache, F. Ferrari, R.A. Yunes, R.J. Nunes, H. Terenzi, B. Botta, M. Botta, PLoS One 8 (2013) e77081.
[13] A. Nören-Müller, W. Wilk, K. Saxena, H. Schwalbe, M. Kaiser, H. Waldmann, Angew. Chem. Int. Ed. 47 (2008) 5973–5977.
[14] A. Noren-Muller, I. Reis-Correa Jr., H. Prinz, C. Rosenbaum, K. Saxena, H.J. Schwalbe, D. Vestweber, G. Cagna, S. Schunk, O. Schwarz, H. Schiewe, H. Waldmann, Proc. Natl. Acad. Sci. USA 103 (2006) 10606–10611.
[15] M.B. Soellner, K.A. Rawls, C. Grundner, T. Alber, J.A. Ellman, J. Am. Chem. Soc. 129 (2007) 9613–9615.
[16] L. Fanzani, F. Porta, F. Meneghetti, S. Villa, A. Gelain, A.P. Lucarelli, E. Parisini, Curr. Med. Chem. 22 (2015) 3110–3132.
[17] Y. He, J. Xu, Z.H. Yu, A.M. Gunawan, L. Wu, L. Wang, Z.Y. Zhang, J. Med. Chem. 56 (2013) 832–842.
[18] L.P. Tan, H. Wu, P.Y. Yang, K.A. Kalesh, X. Zhang, M. Hu, R. Srinivasan, S.Q. Yao,

Org. Lett. 11 (2009) 5102–5105.
[19] L.F. Zeng, J. Xu, Y. He, R. He, L. Wu, A.M. Gunawan, Z.Y. Zhang, ChemMedChem 8 (2013) 904–908.
[20] Z.Y. Zhang, Acc. Chem. Res. 50 (2017) 122–129.
[21] C. Grundner, D. Perrin, R. Hooft van Huijsduijnen, D. Swinnen, J. Gonzalez, C.L. Gee, T.N. Wells, T. Alber, Structure 15 (2007) 499–509.
[22] A. Lavecchia, C. Di Giovanni, Curr. Med. Chem. 20 (2013) 2839–2860.
[23] C.A. Lipinski, F. Lombardo, B.W. Dominy, P.J. Feeney, Adv. Drug Deliv. Rev. 23 (1997) 3–25.
[24] D.F. Veber, S.R. Johnson, H.Y. Cheng, B.R. Smith, K.W. Ward, K.D. Kopple, J. Med. Chem. 45 (2002) 2615–2623.
[25] Y. Lu, M. Zheng, B. Wang, L. Fu, W. Zhao, P. Li, J. Xu, H. Zhu, H. Jin, D. Yin, H. Huang, A.M. Upton, Z. Ma, Antimicrob. Agents Chemother. 55 (2011) 5185–5193.
[26] S.D. Roughley, A.M. Jordan, J. Med. Chem. 54 (2011) 3451–3479.